

Topological basis for understanding the behavior of the heavy-fermion metal $\beta - \text{YbAlB}_4$ under application of magnetic field and pressure

V. R. Shaginyan,^{1,2,*} A. Z. Msezane,² K. G. Popov,^{3,4} J. W. Clark,^{5,6} V. A. Khodel,^{7,5} and M. V. Zverev^{7,8}

¹*Petersburg Nuclear Physics Institute, NRC Kurchatov Institute, Gatchina, 188300, Russia*

²*Clark Atlanta University, Atlanta, GA 30314, USA*

³*Komi Science Center, Ural Division, RAS, Syktyvkar, 167982, Russia*

⁴*Department of Physics, St.Petersburg State University, Russia*

⁵*McDonnell Center for the Space Sciences & Department of Physics, Washington University, St. Louis, MO 63130, USA*

⁶*Centro de Ciências Matemáticas, Universidade de Madeira, 9000-390 Funchal, Madeira, Portugal*

⁷*NRC Kurchatov Institute, Moscow, 123182, Russia*

⁸*Moscow Institute of Physics and Technology, Dolgoprudny, Moscow District 141700, Russia*

Informative recent measurements on the heavy-fermion metal $\beta - \text{YbAlB}_4$ performed with applied magnetic field and pressure as control parameters are analyzed with the goal of establishing a sound theoretical explanation for the inferred scaling laws and non-Fermi-liquid (NFL) behavior, which demonstrate some unexpected features. Most notably, the robustness of the NFL behavior of the thermodynamic properties and of the anomalous $T^{3/2}$ temperature dependence of the electrical resistivity under applied pressure P in zero magnetic field B is at variance with the fragility of the NFL phase under application of a field. We show that a consistent topological basis for this combination of observations, as well as the empirical scaling laws, may be found within fermion-condensation theory in the emergence and destruction of a flat band, and explain that the paramagnetic NFL phase takes place without magnetic criticality, thus not from quantum critical fluctuations. Schematic $T - B$ and $T - P$ phase diagrams are presented to illuminate this scenario.

PACS numbers: 71.27.+a, 71.10.Hf, 72.15.Eb

I. INTRODUCTION

Recent measurements on the heavy-fermion (HF) metal $\beta - \text{YbAlB}_4$ have been performed under the application of both a magnetic field B and hydrostatic pressure P , with results that have received considerable theoretical analysis¹⁻¹⁰. Measurements of the magnetization $M(B)$ at different temperatures T reveal that the magnetic susceptibility $\chi = M/B \propto T^{-1/2}$ demonstrates non-Fermi liquid (NFL) behavior and diverges as $T \rightarrow 0$, implying that the quasiparticle effective mass m^* diverges as $m^* \propto B^{-1/2} \propto T^{-1/2}$ at a quantum critical point (QCP).² This kind of quantum criticality is commonly attributed to scattering of electrons off quantum critical fluctuations related to a magnetic instability; yet in a single crystal of $\beta - \text{YbAlB}_4$, the QCP in question is located well away from a possible magnetic instability, making the NFL phase take place without magnetic criticality.² Additionally, it is observed that the QCP is robust under application of pressure P , in that the divergent T and B dependencies of χ are conserved and are accompanied by an anomalous $T^{3/2}$ dependence of the electrical resistivity ρ .⁶ In contrast to resilience of these divergences under pressure, application of even a tiny magnetic field B is sufficient to suppress them, leading to Landau Fermi liquid (LFL) behavior at low temperatures^{1,2}. Thus, among other unusual features, the metal $\beta - \text{YbAlB}_4$ presents challenging theoretical problems: How to reconcile the frailty of its NFL behavior under application of a magnetic field, with the robustness of the NFL phase against application of pressure

in zero magnetic field; How to explain that the paramagnetic NFL phase takes place without magnetic criticality, thus not from quantum critical fluctuations.

II. SCALING BEHAVIOR

To address these challenges within a topological scenario based on the emergence of a fermion condensate (FC), we begin with an examination of the scaling behavior of the thermodynamic functions of this HF compound considered as homogeneous HF liquid¹¹⁻¹³. We note that the existence of FC has been convincingly demonstrated by purely theoretical and experimental arguments, see e.g.¹⁴⁻¹⁸. The Landau functional $E(n)$ representing the ground-state energy depends on the quasiparticle momentum distribution $n_\sigma(\mathbf{p})$. Near the fermion-condensation quantum phase transition (FC-QPT), the effective mass m^* is governed by the Landau equation^{11,12,20}

$$\frac{1}{m^*(T, B)} = \frac{1}{m^*(T=0, B=0)} + \frac{1}{p_F^2} \sum_{\sigma_1} \int \frac{\mathbf{p}_F \mathbf{p}_1}{p_F} F_{\sigma, \sigma_1}(\mathbf{p}_F, \mathbf{p}_1) \frac{\partial \delta n_{\sigma_1}(T, B, \mathbf{p}_1)}{\partial \mathbf{p}_1} \frac{d\mathbf{p}_1}{(2\pi)^3}, \quad (1)$$

here written in terms of the deviation $\delta n_\sigma(\mathbf{p}) \equiv n_\sigma(\mathbf{p}, T, B) - n_\sigma(\mathbf{p}, T=0, B=0)$ of the quasiparticle distribution from its field-free value under zero pressure. The Landau interaction $F(\mathbf{p}_1, \mathbf{p}_2) = \delta^2 E / \delta n(\mathbf{p}_1) \delta n(\mathbf{p}_2)$ serves to bring the system to the FCQPT point where

$m^* \rightarrow \infty$ at $T = 0$. As this occurs, the topology of the Fermi surface is altered, with the effective mass m^* acquiring temperature and field dependencies such that the proportionalities $C/T \sim \chi \sim m^*(T, B)$ relating the specific heat ratio C/T and the magnetic susceptibility χ to m^* persist. Approaching the FCQPT, $m^*(T = 0, B = 0) \rightarrow \infty$ and thus Eq. (1) becomes homogeneous, i.e., $m^*(T = 0, B) \propto B^{-z}$ and $m^*(T, B = 0) \propto T^{-z}$, with z depending on the analytical properties of F .^{11–13,21} On the ordered side of the FCQPT at $T = 0$, the single-particle spectrum $\varepsilon(\mathbf{p})$ becomes flat in some interval $p_i < p_F < p_f$ surrounding the Fermi surface at p_F , coinciding there with the chemical potential μ ,

$$\varepsilon(\mathbf{p}) = \mu. \quad (2)$$

At the FCQPT the flat interval shrinks, so that $p_i \rightarrow p_F \rightarrow p_f$, and $\varepsilon(\mathbf{p})$ acquires an inflection point at p_F , with $\varepsilon(\mathbf{p} \simeq \mathbf{p}_F) - \mu \simeq (p - p_F)^3$. Another inflection point emerges in the case of a non-analytical Landau interaction F , instead with

$$\begin{aligned} \varepsilon - \mu &\simeq -(p_F - p)^2, p < p_F \\ \varepsilon - \mu &\simeq (p - p_F)^2, p > p_F \end{aligned} \quad (3)$$

at which the effective mass diverges as $m^*(T \rightarrow 0) \propto T^{-1/2}$. Such specific features of ε can be used to identify the solutions of Eq. (1) corresponding to different experimental situations. In particular, the experimental results obtained for $\beta - \text{YbAlB}_4$ show that near QCP at $B \simeq 0$, the magnetization obeys^{1–10} $M(B) \propto B^{-1/2}$. This behavior corresponds to the spectrum $\varepsilon(\mathbf{p})$ given by Eq. (3) with $(p_f - p_i)/p_F \ll 1$. At finite B and T near the FCQPT, the solutions of Eq. (1) determining the T and B dependencies of $m^*(T, B)$ can be well approximated by a simple universal interpolating function^{11–13}. The interpolation occurs between the LFL ($m^* \propto a + bT^2$) and NFL ($m^* \propto T^{-1/2}$) regimes separated by the crossover region at which m^* reaches its maximum value m_N^* at temperature T_M , and represents the universal scaling behavior of

$$m_N^*(T_N) = \frac{m^*(T, B)}{m_M^*} = \frac{1 + c_2}{1 + c_1} \frac{1 + c_1 T_N^2}{1 + c_2 T_N^{5/2}}. \quad (4)$$

Here c_1 and c_2 are fitting parameters, $T_N = T/T_M$ is the normalized temperature, and

$$m_M^* \propto B^{-1/2}, \quad (5)$$

while

$$T_M \propto B^{1/2} \text{ and } T_M \propto B. \quad (6)$$

It follows from Eqs. (4), (5), and (6) that the effective mass exhibits the universal scaling behavior

$$m^*(T, B) = c_3 \frac{1}{\sqrt{B}} m_N^*(T/B), \quad (7)$$

with c_3 a constant.^{11–13} Eqs. (4), (5), (6), and (7) will be used along with Eq. (1) to account for the experimental observations on $\beta - \text{YbAlB}_4$. We note that the scaling behavior at issue refers to temperatures $T \lesssim T_f$, where T_f is the temperature at which the influence of the QCP becomes negligible.^{11,12}

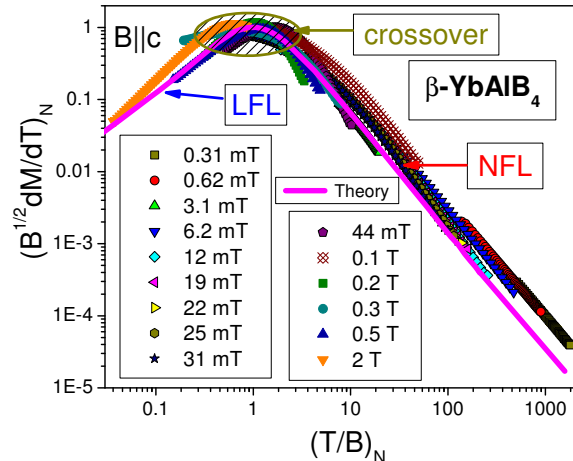


FIG. 1: (color online). Scaling behavior of dimensionless normalized magnetization $(B^{1/2} dM(T, B)/dT)_N$ versus dimensionless normalized $(T/B)_N$ at magnetic field values B given in the legend. Data are extracted from the measurements described in Ref. 6. Regions of LFL behavior, crossover, and NFL behavior are indicated by arrows. The theoretical prediction is represented by a single scaling function.

Based on Eq. (7), we conclude the magnetization M as described within the topological setting of fermion condensation does exhibit the empirical scaling behavior, being given by

$$M(T, B) = \int \chi(T, B_1) dB_1 \propto \int \frac{m_N^*(T/B_1)}{\sqrt{B_1}} dB_1. \quad (8)$$

At $T < B$ the system is predicted to show LFL behavior with $M(B) \propto B^{-1/2}$, whereas at $T > B$, the system has entered the NFL region and $M(T) \propto T^{-1/2}$. Moreover, $dM(T, B)/dT$ again exhibits the observed scaling behavior, with $dM(T, B)/dT \propto T$ at $T < B$ and $dM(T, B)/dT \propto T^{-3/2}$ at $T > B$. Thus our analytical results are in accordance experiment,^{2,4,5} free from fitting parameters and empirical functions.

In confirmation of the analysis of the scaling behavior, Fig. 1 displays our calculations of the dimensionless normalized magnetization measure $(B^{1/2} dM(T, B)/dT)_N$ versus the dimensionless normalized ratio $(T/B)_N$. The normalization is implemented by dividing $B^{1/2} dM(T, B)/dT$ and T/B respectively by the maximum value of $(B^{1/2} dM(T, B)/dT)_M$ and by the value of $(B/T)_M$ value the maximum occurs. It is seen that the calculated single scaling function of the

ratio $(T/B)_N$ tracks the data over four decades of the normalized quantity $(B^{1/2}dM(T,B)/dT)_N$, while the ratio itself varies over five decades. It also follows from Eq. (8) that $(B^{1/2}dM(T,B)/dT)_N$ exhibits the proper scaling behavior as a function of $(B/T)_N$. Figure 2 illustrates the scaling behavior $(B^{1/2}dM(T,B)/dT)_N$ of the archetypal HF metal YbRh_2Si_2 . The solid curve representing the theoretical calculations is taken from Fig. 1. Thus, we find that the scaling behavior of $\beta - \text{YbAlB}_4$, as extracted from measurements^{22,23} and shown in Fig. 1, is not unique, as Fig. 2 demonstrates the same crossover under application of the magnetic field in the wide range of the applied pressure.

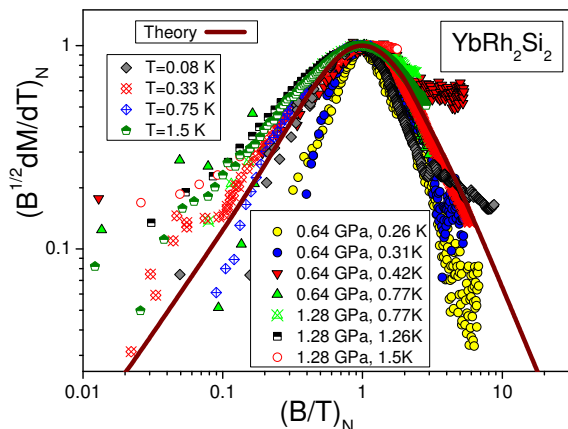


FIG. 2: (color online). Scaling behavior of the archetypal HF metal YbRh_2Si_2 . Data for $(B^{1/2}dM(T,B)/dT)_N$ versus $(B/T)_N$ are extracted from measurements of dM/dT versus B at fixed temperatures.^{22,23} The solid curve representing the theoretical calculation is adapted from that of Fig. 1. Applied pressures and temperatures are shown in the legends.

III. THE KADOWAKI-WOODS RATIO

Under application of magnetic fields $B > B_{c2} \simeq 30$ mT and at sufficiently low temperatures, $\beta - \text{YbAlB}_4$ can be driven to the LFL state having resistivity of the form $\rho(T) = \rho_0 + AT^2$. Measurements of the coefficient A of the T^2 dependence have provided information on its B -field dependence¹. Being proportional to the quasiparticle-quasiparticle scattering cross section, $A(B)$ is found to obey^{24,25} $A \propto (m^*(B))^2$. In accordance with Eq. (5), this implies that

$$A(B) \simeq A_0 + \frac{D}{B}, \quad (9)$$

where A_0 and D are fitting parameters.^{11,12} We rewrite Eq. (9) in terms of the reduced variable A/A_0 ,

$$\frac{A(B)}{A_0} \simeq 1 + \frac{D_1}{B}, \quad (10)$$

where $D_1 = D/A_0$ is a constant, thereby reducing $A(B)$ to a function of the single variable B . Figure 3 presents the fit of $A(B)$ to the experimental data.¹ The theoret-

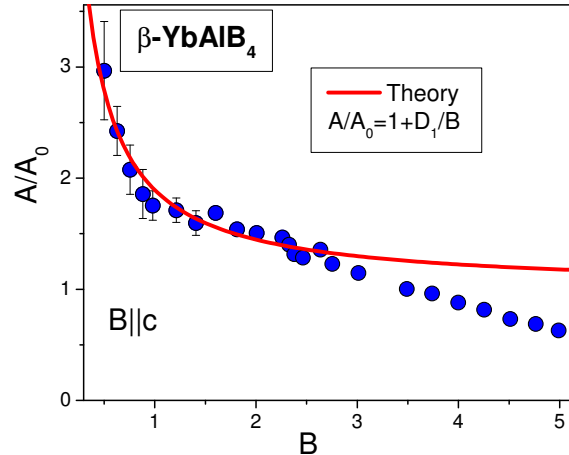


FIG. 3: (color online). Experimental data for normalized coefficient $A(B)/A_0$ as represented by Eq. (10), plotted as a function of magnetic field B (solid circles). Measured values of $A(B)$ are taken from Ref. 1, with D_1 the only fitting parameter. The solid curve is the theoretical prediction.

ical dependence (10) agrees well with experiment over a substantial range in B . This concurrence suggests that the physics underlying the field-induced re-entrance into LFL behavior is the same for classes of HF metals. It is important to note here that deviations of the theoretical curve from the experimental points at $B > 2.5$ T are due to violation of the scaling at the QCP.⁵

Fig. 4 compares our calculations of $\chi(B) \propto m^*$ and $C/T = \gamma(B) \propto m^*$ with the experimental measurements.⁵ Appealing to Eq. (5), the behavior $A(B) \propto (m^*)^2$, and the good agreement of theory with experiment shown in this figure, we verify Eq. (10) and conclude that the Kadowaki-Woods ratio $A/\gamma^2 \propto A/\chi^2 \simeq \text{const.}$ is conserved in the case of $\beta - \text{YbAlB}_4$, much as in other heavy-fermion compounds^{1,3,11,26}.

IV. THE PHASE DIAGRAMS

The results of the above analysis of the scaling properties of this HF system based on a topological scenario allow us to construct the schematic $T - B$ phase diagram of $\beta - \text{YbAlB}_4$ presented in Fig. 5, with the magnetic field B as control parameter. At $B = 0$, the system acquires

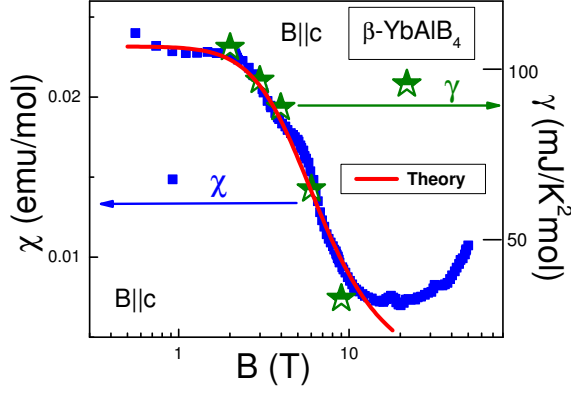


FIG. 4: (color online). Measurements⁵ of magnetic susceptibility $\chi = dM/dB = a_1 m_N^*$ (left axis, square data points) and electronic specific heat coefficient $C/T = \gamma = a_2 m_N^*$ (right axis, stars), plotted versus magnetic field B . Solid curve tracing scaling behavior of m_N^* : theoretical results from present study with fitting parameters a_1 and a_2 .

a flat band satisfying Eq. (2), implying the presence of a fermion condensate in a strongly degenerate state of matter that becomes susceptible to transition into a superconducting state^{11,27}. This NFL fermion-condensate regime exists at elevated temperatures and fixed magnetic field. QCP indicated by the arrow in Fig. 5 is located at the origin of the phase diagram, since application of any magnetic field destroys the flat band and shifts the system into the LFL state, *provided* that the superconducting state is not in play^{11,12,28}. The hatched area in the figure denotes the crossover region that separates the NFL state from the LFL state, also indicated in Fig. 1.

Significantly, the heavy-fermion metal $\beta - \text{YbAlB}_4$ is in fact a superconductor on the ordered side of the corresponding phase transition. When analyzing the NFL behavior of $\rho(T)$ on the disordered side of this transition, it should be kept in mind that several bands simultaneously intersect the Fermi surface, so that the HF band never covers the entire Fermi surface. Accordingly, it turns out that quasiparticles that do not belong to the HF band make the main contribution to the conductivity. The resistivity therefore takes the form $\rho(T) = m_{\text{norm}}^* \gamma(T)$, where m_{norm}^* is the average effective mass of normal quasiparticles and $\gamma(T)$ describes their damping. The main contribution to $\gamma(T)$ can be estimated as^{29–32} $\gamma \propto T^2 m^* (m_{\text{norm}}^*)^2$. Based on Eqs. (3) and (6), we obtain³² $\rho(T) \propto T^{3/2}$. On the other hand, one would expect that at $T \rightarrow 0$ the flat band (2) comes into play, producing the behavior $\rho(T) \propto A_1 T$, with the factor A_1 proportional to the flat-band range $(p_f - p_i)/p_F \ll 1$. However, such behavior is not seen, because this area of the phase diagram is captured by superconductivity, as already indicated in Fig. 5. The low- T resistivity $\rho(T, P = 0) \propto T^{3/2}$ found experimentally⁶

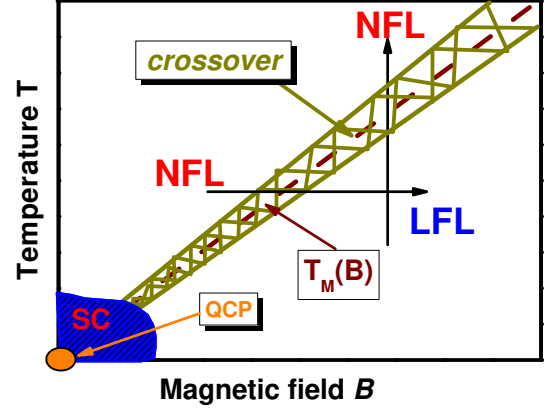


FIG. 5: Schematic $T - B$ phase diagram. Vertical and horizontal arrows highlight LFL-NFL and NFL-LFL transitions at fixed B and T , respectively. Hatched area separates the NFL phase from the weakly polarized LFL phase and identifies the transition region. Dashed line in hatched area represents the function $T_M \propto B$ (see Eq. (6)). The QCP, located at the origin and indicated by the arrow, is the quantum critical point at which the effective mass m^* diverges. It is surrounded by the superconducting phase labeled SC.

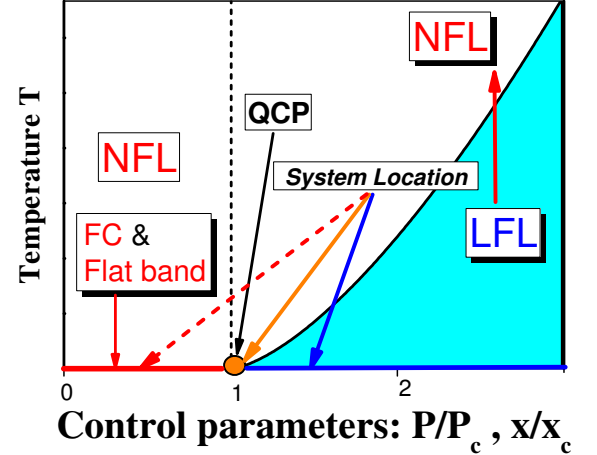


FIG. 6: Schematic $T - x$ phase diagram of HF system exhibiting a fermion condensate. Pressure P/P_c and number-density index x/x_c are taken as control parameters, with x_c the critical doping. At $P/P_c > 1$ and sufficiently low temperatures, the system is located in the LFL state (shaded area). Moving past the QCP point to $P/P_c < 1$ into the NFL region, the system develops a flat band that is the signature of fermion condensation (FC). The upward vertical arrow tracks the system moving in the LFL-NFL direction along T at fixed control parameters. Not shown is the low-temperature stable phase satisfying the Nernst theorem (superconducting in the case of $\beta - \text{YbAlB}_4$) that must exist for P/P_c or x/x_c below unity.

for the normal state of $\beta - \text{YbAlB}_4$ is consistent with this analysis. When the pressure P is raised to a critical value P_c , there is a crossover to Landau-like behavior $\rho(T) = \rho_0 + A_2 T^2$. Assuming that $P \propto x$, where x is the doping or the HF number density,²³ we observe that such behavior closely resembles the NFL behavior $\rho(T) \propto T^{1.5 \pm 0.1}$ revealed in measurements of the resistivity in the electron-doped high- T_c superconductors $\text{La}_{2-x}\text{Ce}_x\text{CuO}_4$.^{33,34} In that case the effective mass $m^*(x)$ diverges as $x \rightarrow x_c$ or $P \rightarrow P_c$ ^{33,34} according to^{11,12,32}

$$(m^*(x))^2 \propto A \simeq \left(a_1 + \frac{a_2}{x/x_c - 1} \right)^2. \quad (11)$$

Here a_1 and a_2 are constants, while x_c is the critical doping at which the NFL behavior changes to LFL behavior, the FC having decayed at x_c and the system having moved to the disordered side of the FCQPT.

In Fig. 6 we display the schematic $T-x$ phase diagram exhibited by $\beta - \text{YbAlB}_4$ when the system is tuned by pressure P or by number density x . At $P/P_c < 1$ (or $x/x_c < 1$) the system is located on the ordered side of topological phase transition FCQPT and demonstrates NFL behavior at $T \lesssim T_f$. Thus, the NFL behavior induced by the FC that persists at $P < P_c$ is robust under application of pressure $P/P_c < 1$.^{12,28} (We note that such behavior is also observed in quasicrystals.^{13,35}) At low temperatures the FC state possessing a flat band, highlighted in the figure, is strongly degenerate. This degeneracy stimulates the onset of certain phase transitions and is thereby lifted before reaching $T = 0$, as required by the Nernst theorem.^{27,36} With rising pressure (indi-

cated by arrows in Fig. 6), the system enters the region $P/P_c > 1$, where it is situated prior to the onset of the FCQPT and demonstrates LFL behavior at sufficiently low temperatures (shaded area in the figure). The temperature range of this region shrinks when $P/P_c \rightarrow 1$, and m^* diverges as described by Eq. (11). These observations are in accord with the experimental evidence.⁶

V. SUMMARY

To summarize, we have analyzed the thermodynamic properties of the heavy-fermion metal $\beta - \text{YbAlB}_4$ and explained their enigmatic scaling behavior within a topological scenario in which FC phase plays an essential role. We have explained why the observed NFL behavior is extremely sensitive to a magnetic field, and how the thermodynamic properties and anomalous $T^{3/2}$ dependence of the electrical resistivity remain intact under the application of a pressure.

VI. ACKNOWLEDGMENTS

VRS acknowledges support from the Russian Science Foundation, Grant No. 14-22-00281. This research was also supported by RFBR Grants #14-02-00044 and 15-02-06261, and by grant NS-932.2014.2 from the Russian Ministry of Sciences (MVZ and VAK). VAK and JWC thank the McDonnell Center for the Space Sciences for timely support.

* Electronic address: vrshag@thd.pnpi.spb.ru

¹ S. Nakatsuji, K. Kuga, Y. Machida, T. Tayama, T. Sakakibara, Y. Karaki, H. Ishimoto, S. Yonezawa, Y. Maeno, E. Pearson, G. G. Lonzarich, L. Balicas, H. Lee, and Z. Fisk, *Nat. Phys.* **4**, 603 (2008).

² Y. Matsumoto, S. Nakatsuji, K. Kuga, Y. Karaki, N. Horie, Y. Shimura, T. Sakakibara, A. H. Nevidomskyy, and P. Coleman, *Science* **331**, 316 (2011).

³ Y. Matsumoto, K. Kuga, T. Tomita, Y. Karaki, and S. Nakatsuji, *Phys. Rev. B* **84**, 125126 (2011).

⁴ Y. Matsumoto, S. Nakatsuji, K. Kuga, Y. Karaki, Y. Shimura, T. Sakakibara, A. H. Nevidomskyy, and P. Coleman, *J. Phys.: Conf. Ser.* **391**, 012041 (2012).

⁵ Y. Matsumoto, K. Kuga, Y. Karaki, Y. Shimura, T. Sakakibara, M. Tokunaga, K. Kindo, and S. Nakatsuji, *J. Phys. Soc. Jpn.* **84**, 024710 (2015).

⁶ T. Tomita, K. Kuga, Y. Uwatoko, P. Coleman, S. Nakatsuji, *Science* **349**, 506 (2015).

⁷ A. H. Nevidomskyy and P. Coleman, *Phys. Rev. Lett.* **102**, 077202 (2009).

⁸ A. Ramires, P. Coleman, A. H. Nevidomskyy, and A. M. Tsvelik, *Phys. Rev. Lett.* **109**, 176404 (2012).

⁹ S. Watanabe and K. Miyake, *J. Phys. Soc. Jpn.* **82**, 083704 (2013).

¹⁰ S. Watanabe and K. Miyake, *J. Phys. Soc. Jpn.* **83**, 103708 (2014).

¹¹ V. R. Shaginyan, M. Ya. Amusia, A. Z. Msezane, and K. G. Popov, *Phys. Rep.* **492**, 31 (2010).

¹² M. Ya. Amusia, K. G. Popov, V. R. Shaginyan, V. A. Stephanovich, *Theory of Heavy-Fermion Compounds*, Springer Series in Solid-State Sciences **182**, Cham, Heidelberg, New York, Dordrecht, London (2014).

¹³ V. R. Shaginyan, A. Z. Msezane, K. G. Popov, G. S. Japaridze, and V. A. Khodel, *Phys. Rev. B* **87**, 245122 (2013).

¹⁴ D. Lidsky, J. Shiraishi, Y. Hatsugai, and M. Kohmoto, *Phys. Rev. B* **57**, 1340 (1998).

¹⁵ S.-S. Lee, *Phys. Rev. D* **79**, 086006 (2009).

¹⁶ D. Yudin, D. Hirschmeier, H. Hafermann, O. Eriksson, A. I. Lichtenstein, and M. I. Katsnelson, *Phys. Rev. Lett.* **112**, 070403 (2014).

¹⁷ G. E. Volovik, *Phys. Scr.* **T164**, 014014 (2015).

¹⁸ A.A. Shashkin, V.T. Dolgoplov, J.W. Clark, V.R. Shaginyan, M.V. Zverev, and V.A. Khodel, *Phys. Rev. Lett.* **112**, 186402 (2014).

¹⁹ M. Yu. Melnikov, A. A. Shashkin, V. T. Dolgoplov, S.-H. Huang, C. W. Liu, and S. V. Kravchenko, arXiv:1604.08527.

- ²⁰ L. D. Landau, Sov. Phys. JETP **3**, 920 (1956).
- ²¹ V. A. Khodel, V. R. Shaginyan, and V. V. Khodel, Phys. Rep. **249**, 1 (1994).
- ²² Y. Tokiwa, T. Radu, C. Geibel, F. Steglich, and P. Gegenwart, Phys. Rev. Lett. **102**, 066401 (2009).
- ²³ Y. Tokiwa, P. Gegenwart, C. Geibel, and F. Steglich, J. Phys. Soc. Jpn. **78**, 123708 (2009).
- ²⁴ V.A. Khodel and P. Schuck, Z. Phys. B: Condens. Matter **104**, 505 (1997).
- ²⁵ P. Gegenwart, J. Custers, C. Geibel, K. Neumaier, T. Tayama, K. Tenya, O. Trovarelli, and F. Steglich Phys. Rev. Lett. **89**, 056402 (2002).
- ²⁶ K. Kadowaki and S. B. Woods, Solid State Commun. **58**, 507 (1986).
- ²⁷ V.A. Khodel, J.W. Clark, and M.V. Zverev, Phys. Rev. B **78**, 075120 (2008).
- ²⁸ V. R. Shaginyan, A. Z. Msezane, K. G. Popov, G. S. Japaridze, and V. A. Khodel, Europhys. Lett. **106**, 37001 (2014).
- ²⁹ V. A. Khodel and M. V. Zverev, JETP Lett. **85**, 404 (2007).
- ³⁰ V. R. Shaginyan, A. Z. Msezane, K. G. Popov, J. W. Clark, M. V. Zverev, and V. A. Khodel, Phys. Rev. B **86**, 085147 (2012).
- ³¹ V. A. Khodel, V. R. Shaginyan, and P. Schuck, JETP Lett. **63**, 752 (1996).
- ³² V. A. Khodel, J. W. Clark, K. G. Popov, and V. R. Shaginyan, JETP Lett. **101**, 413 (2015).
- ³³ N. P. Armitage, P. Fournier, and R. L. Greene, Rev. Mod. Phys. **82**, 2421 (2010).
- ³⁴ K. Jin, N. P. Butch, K. Kirshenbaum, J. Paglione, and R. L. Greene, Nature, **476**, 73 (2011).
- ³⁵ K. Deguchi, S. Matsukawa, N. K. Sato, T. Hattori, K. Ishida, H. Takakura, and T. Ishimasa, Nature Materials **11**, 1013 (2012).
- ³⁶ J. W. Clark, M. V. Zverev, and V. A. Khodel, Ann. Phys. **327**, 3063 (2012).